Journal of Fluids and Structures (1998) **12,** 183–196

THE SLAM FORCE ON A FLAT PLATE IN FREE FLIGHT DUE TO IMPACT ON A WAVE CREST

N. J. Smith, P. K. Stansby and J. R. Wright

Manchester School of Engineering, The University of Manchester, Manchester M13 9PL, U.K.

(Received 12 February 1997 and in revised form 22 October 1997)

An experimental investigation of the maximum vertical force on a flat plate in free flight due to impact on water waves has been made. The plate is horizontal and impacts a wave crest at mid-length. The mass, impact velocity, flight path angle and wave steepness were varied. A slam force coefficient based on dimensional concepts and physical reasoning is produced which is well described by a formula which omits the effects of acceleration due to gravity, water and air compressibility and surface tension. High-speed video was used to visualize the jets produced at impact, showing them to have high velocity and a fine droplet structure.

1. INTRODUCTION

There are many situations when a moving body hits water, suffering loss of momentum, vibration, structural deformation and noise generation. This is particularly marked for bodies in free flight ranging from life-boat launching to various ditching scenarios, e.g. aircraft, helicopters, escape and space capsules. There are similar experiences when high-speed marine vessels, such as surface effect ships, hydrofoils, hovercraft and catarmarans, hit surface waves. The loading is very high in all cases and in the ditching scenario represents one of the most severe loading cases for determining structural integrity. For high-speed craft, it is necessary to assess the effect of repetitive impact loading on fatigue life and ride comfort. The fundamental flow mechanisms which generate the impact force are similar in all cases and have received intermittent attention over the years through theoretical, experimental and numerical analysis. In addition, over the past decade, wave slam loading on offshore structures has had important design implications, both in relation to wet deck slamming and wave breaking on cylindrical elements.

Theories have been developed to predict slam forces assuming incompressible, inviscid flow, ignoring gravity. The first study was probably by von Karman (1929) in relation to seaplane landing. He considered the body to be a circular cylinder, representing its immersion as an expanding flat plate with the water surface remaining flat. This approach was extended by Wagner (1932) for the wedge-entry problem by incorporating some local jet analysis. Self-similar solutions for wedge entry have been produced by Do-brovol'skaya (1969). These theories have been applied by Greenhow & Yanbao (1987) to the cylinder slamming problem, showing reasonable agreement with experiment. The approach ignoring free-surface distortion has been generalized by Cooker & Peregrine (1995) using the pressure impulse function and has been applied to wet deck slamming by Wood & Peregrine

0889-9746/98/020183 + 14 $25.00/fl970132

(1996). Gravity and advection may be incorporated in numerical solutions through time-stepping boundary-integral methods for nonlinear potential-flow problems, directly resolving the thin jets produced at impact [e.g. Greenhow (1987), Zhao & Faltinsen (1993)]. Zhao & Faltinsen (1992) have applied all three theoretical approaches (asymptotic, similarity and boundary-element methods) to slam loads on wedges with deadrise angles between 4° and 81°. The asymptotic method was generalized to approximate wet deck slamming on high-speed vessels in waves and showed the importance of wave slope. The importance of slamming loads on the vertical acceleration of a vessel was clearly demonstrated.

The case of a circular jet impacting a solid surface has been analysed by Korobkin (1996) giving the pressure distribution behind the shock front produced in the jet. It was conjectured that the fine structure of the spray jets will give an indication of the physical processes involved, but the spray jets themselves will have little effect on the forces generated. While this last point is consistent with pressure-impulse theory, its neglect of compressible effects could be significant in certain situations. The incorporation of surface tension in theoretical models has not been attempted, to our knowledge, although the effect of entrained air on slam forces has been assessed by Peregrine & Thais (1996).

Relevant experimental work dates back to Batterson (1951), who investigated forces on rectangular skis for use as landing devices on aircraft. In the U.K. there have been investigations of seaplane landing loads specified by the Civil Aviation Authority in the British Airworthiness Requirements. This is used for hovercraft design, with results from full-scale tests on the early hovercraft SRN1 (Crewe 1960) through the British Hovercraft Safety Requirements (1992). There have been further experiments on flat-plate impact: Verhagen (1967) taking account of the compressible layer of air between the plate and the water surface, and Ando (1989) taking account of different plate surfaces and a "cushion" layer attached to the plate.

Although various formulae have been generated and theories applied, the accurate specification of impact loads and decelerations for a body hitting a flat water surface remains problematic and it is uncertain which fluid properties are significant in different situations. The influence of waves is important in many problems but has received little attention.

With this background, an experimental programme has been initiated to study decelerations and hence loads on bodies in free flight hitting water waves. A novel rig has been incorporated in a large wave flume which allows the mass, velocity and flight angle of the body to be varied. The point of impact in a wave cycle is controlled and the wave height and wavelength may be specified. Body acceleration is measured and high-speed video is used to visualize the flow at impact. This paper is concerned with a rigid flat plate of variable width, with side plates to maintain nominally two-dimensional flow. The plate is horizontal in free flight and impacts a crest at mid-length.

2. EXPERIMENTS

The experiments were carried out in a wave flume, 20 m long, 1·2 m wide, with a maximum water depth of about 1 m and glass side panels along its length. Waves were generated by a hinge-type paddle at one end and dissipated on a beach of 1 : 20 slope at the other. In order to launch bodies into the waves, an aluminium frame structure was mounted half-way along the flume. A photograph of the apparatus is shown in Figure 1 and a third angle projection in Figure 2. The two lower parallel channels which are 6 m long act as guide rails for the wheels of the carriage to which the bodies are bolted. The framework was bolted

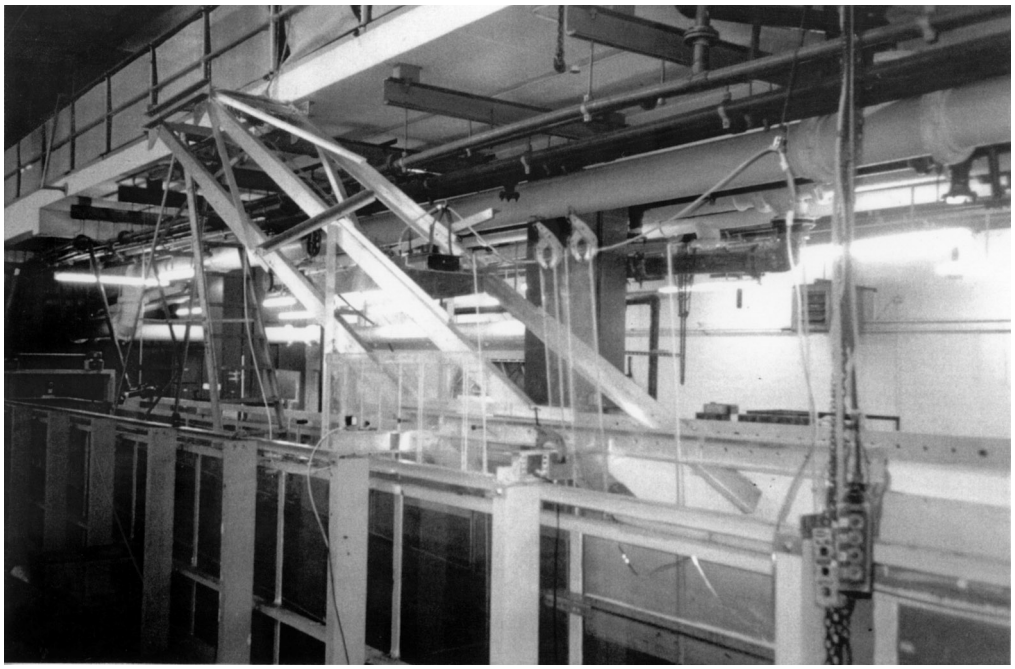

Figure 1. Photograph showing rig and wave flume.

together in such a way that the angle of inclination can be varied from 20 to 90° (vertical) in steps of 10°.

The elevation of the starting position can be varied to control the velocity of the body in free flight. The carriage is released by a pull rod activated by a pneumatic cylinder with an air supply controlled by a solenoid valve. A piezoelectric accelerometer was fitted to the centre of the carriage and connected to a Brüel & Kjaer charge amplifier by a suitably protected cable. The output from the amplifier is recorded by a Cambridge Instruments CED1401 data analyser which is interfaced to a 486 PC. Water surface elevation ahead of the impact zone is measured by two wave probes with output read by the data analyser. The wave height, celerity and wavelength are thus obtained directly and information on the advancing wave profile determines, through a computer program, the release time of the carriage enabling the body to impact the surface at the desired point in the profile, the wave crest in this study. The velocity of the carriage/body at the bottom of the track just before free flight was measured directly by photocell proximity sensors mounted on the rig. After the carriage has been released, at the time the carriage breaks the beam of the photocell sensor, the computer program activates recording of the output signal from the accelerometer at a sampling rate of 10 kHz for 0·3 s. All data are read into the PC memory for analysis.

Three flat aluminium plates with widths of 225, 410 and 565 mm, and 3 mm thick, as shown in Figure 3, were bolted to a box frame below the carriage for testing. Side plates of the same thickness extending 100 mm below the plate were bolted on to the plate to prevent sideways movement of water, that is to keep the flow as two-dimensional as possible in a vertical plane. The box frame supporting a plate was constructed from $38 \times 38 \times 3\,\text{mm}^3$

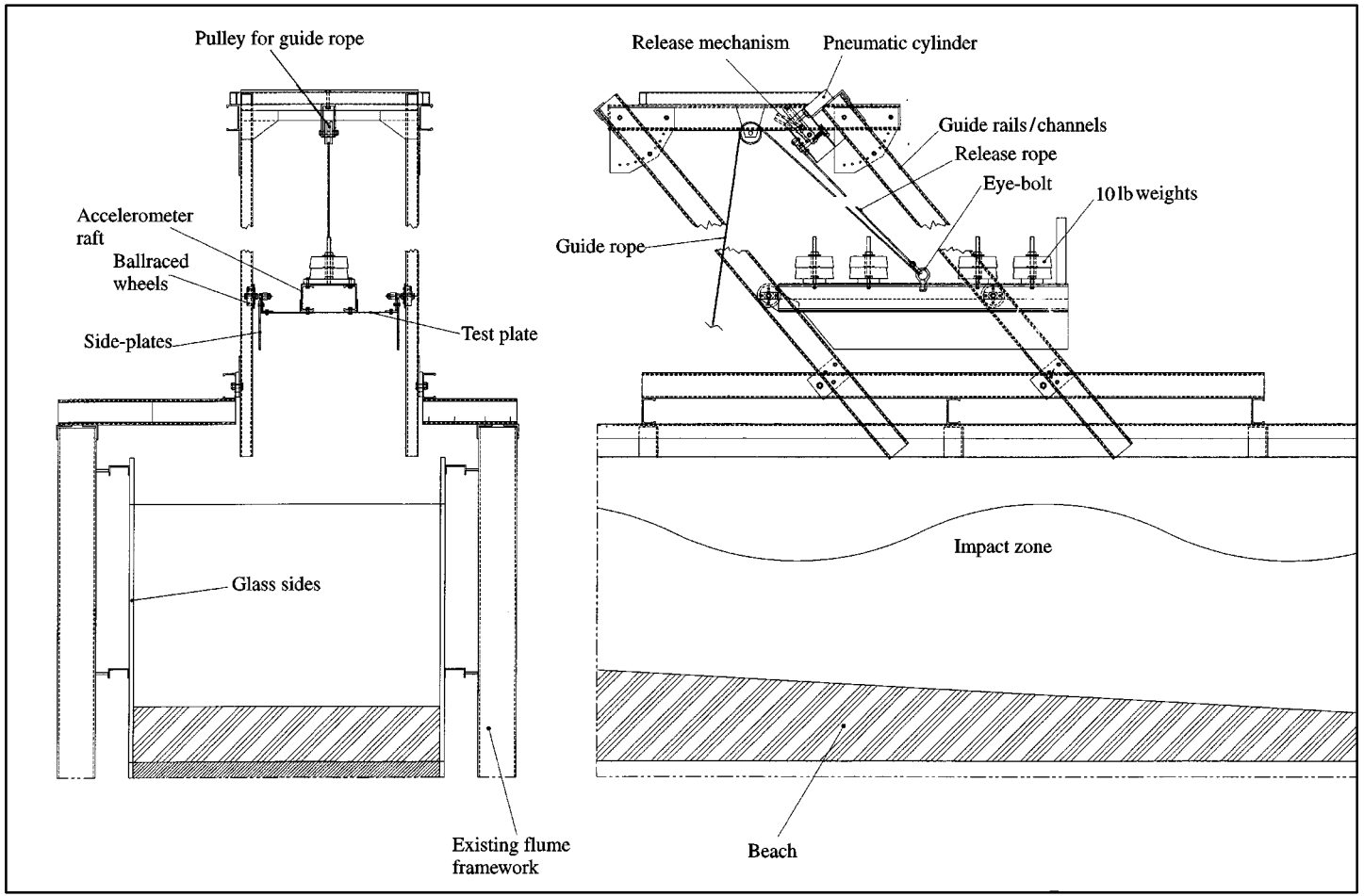

Figure 2. Third-angle projection of wave impact test framework.

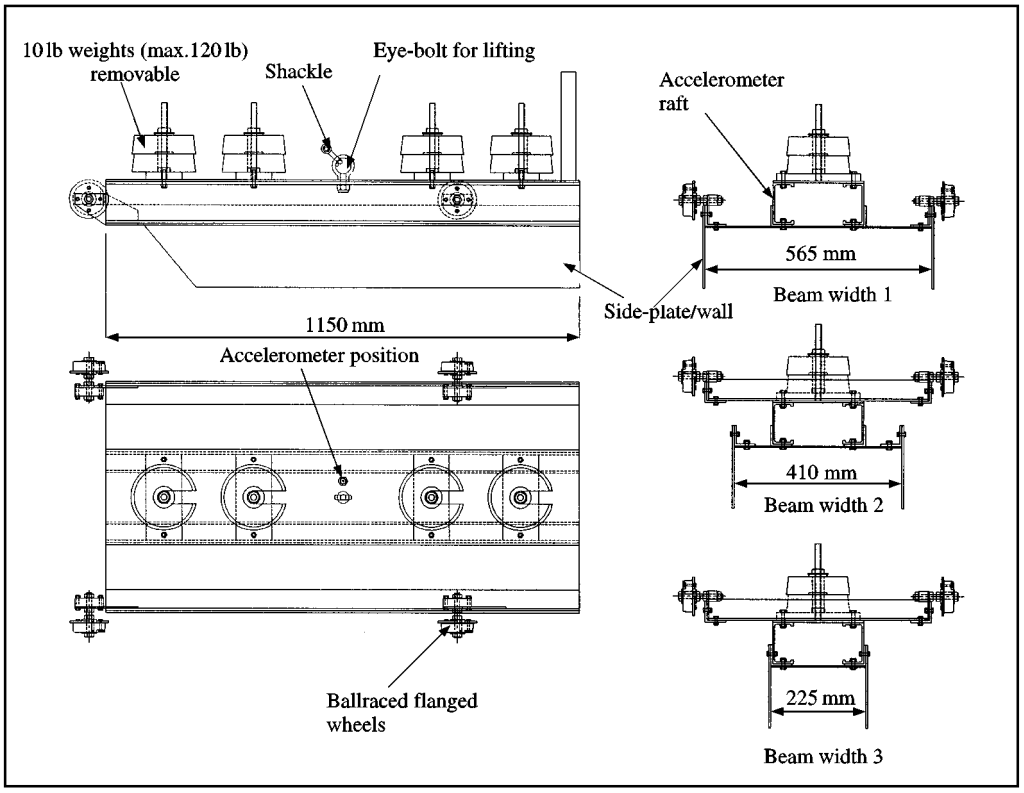

Figure 3. Third-angle projection of flat-plate test-sections (with side plates).

aluminium angles and 3 mm thick aluminium plates as shown in Figure 3. The effective mass of a body was varied by bolting 10 lb (1 kg = 2·20 lb) weights at four points on the top of the carriage (made from steel plates and angles). The carriage and plate support was thus rigidly constructed in an attempt to minimize the effect of vibration on the output from the accelerometer. Aluminium was mainly used to avoid corrosion.

Figure 4 shows an accelerometer time history for a typical plate impact using a low-pass filter in the hardware with frequency cut-offs of 3 kHz, 1 kHz and 100 Hz. The low-frequency vibration modes of the carriage when freely suspended were measured to be much greater than 100 Hz, and all high-frequency content due to structural vibration (although now influenced by the water contact) can be seen to be effectively removed with the 100 Hz cut-off. A check on whether the 100 Hz hardware filter was high enough to capture accurately the body deceleration time history was provided by comparing the displacement obtained by double integration of acceleration time history (see below) with that measured directly from frames of the high-speed video recording. It is also worth mentioning that some tests were made with polypropylene foam layers (25 and 50 mm thick) attached to the underside of the plate. This removed most of the high-frequency oscillation from the accelerometers (and the explosive sound at impact) and slightly increased the peak deceleration (by less than 10%), although the form of the time histories, particularly after peak deceleration, could be quite different (as might be expected due to different buoyancy

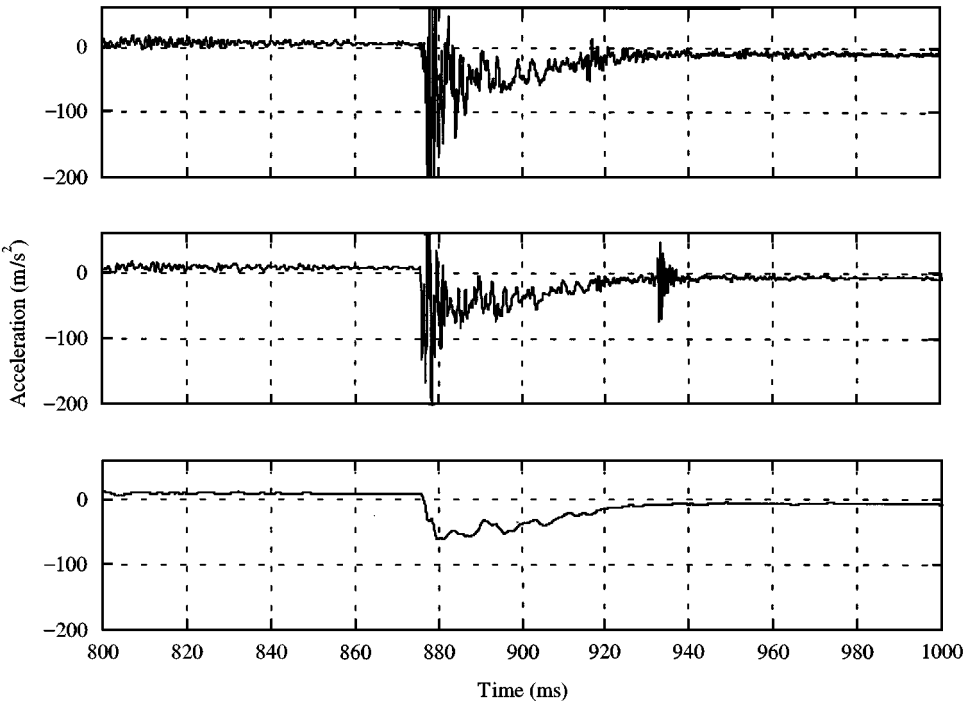

Figure 4. Plot of typical accelerometer output time histories measured during a wave impact. Raw data (a) with 3 kHz hardware low-pass filter; (b) with 1 kHz low-pass filter; (c) with 100 Hz low-pass filter. Flight path angle: 40°.

effects). This further suggests that the peak slam forces measured here are at least only slightly dependent on structural vibration.

A large number of parameter combinations were tested. For each case, the runs were repeated 5–10 times to assess repeatability. A visual check was also provided by a video replay. The experiments were undertaken in the following stages. First, mass was varied in increments of 40 lb up to a maximum of 120 lb for a given wave profile, release height and flight path angle. Second, the impact velocity was varied by changing the release height; three levels were used. The velocity at impact is obtained from the horizontal and vertical components at the bottom of the track, measured by the photocell sensor, added to the vertical component obtained from the integration of acceleration while the body was in free flight. The magnitude of velocity relative to wave motion varied between about 6 and 9 m/s. Third, the beam width was varied; the three values used have been mentioned above. Fourth, the flight path angle was varied by changing the track angle between 20° and 50° in 10° increments. Finally, wave profiles were varied for seven values of H/L in a range between 0 and 0.11, with H between 0 and 0.2 m and L between about 1·5 and 3 m. Overall, 35 different parameter combinations were tested.

A typical acceleration time history is shown in Figure 5 with the resulting vertical velocity and displacement obtained by integration. To show typical repeatability, peak decelerations for 11 runs with four different masses are shown in Table 1 for a track inclination of 40° and $H/L = 0{\cdot}11$. The corresponding averaged acceleration time histories for each mass are shown in Figure 6. The maximum vertical force experienced during impact is simply

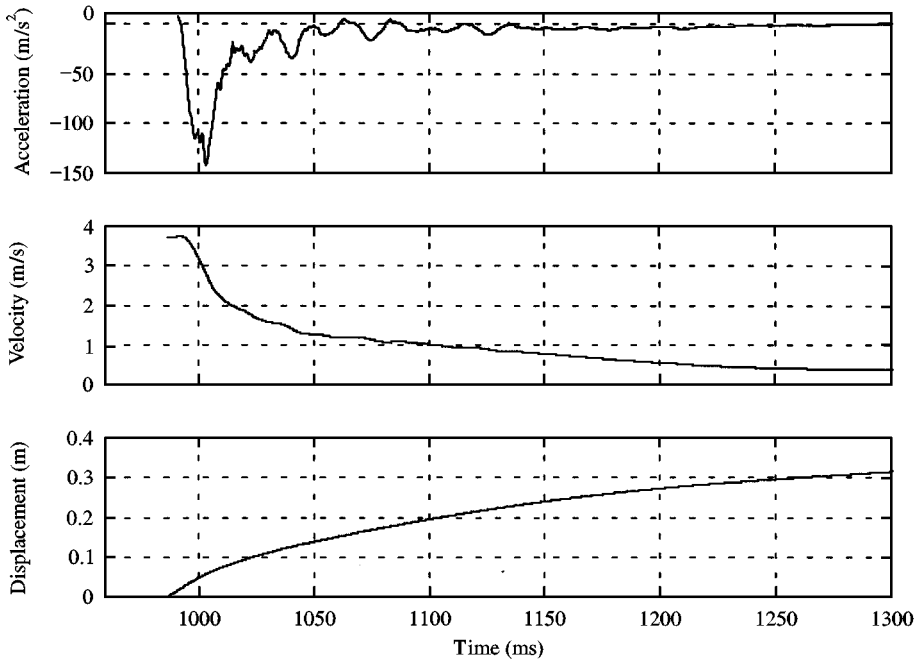

Figure 5. Typical accelerometer time history with resulting vertical velocity and displacement obtained by integration.

TABLE 1
Maximum deceleration for a flat plate of varying mass during wave impacts. Relative velocity = 5·95 m/s; flight path angle = 38°; wave steepness $H/L = 0{\cdot}1$

Run No.	Peak deceleration (m/s²)			
	57 kg	75 kg	93 kg	111 kg
1	124	119·1	97·4	82·3
2	123·8	109·2	98·7	88·7
3	120	110·1	99·6	92·8
4	122·8	105·4	100·2	88·3
5	121·8	101·2	95·8	87·1
6	118·3	109	95·3	90·1
7	119·8	110·8	101·8	89·9
8	129·8	104·8	96·8	91·8
9	114·8	107·8	97·9	91·2
10	117·8	107·2	93·4	89·5
11	122·4	110·7	88·2	86·3
Average	121·4	108·7	96·8	88·9
g	12·37	11·08	9·87	9·06

obtained from the product of the mass and the sum of the peak deceleration and the gravitational acceleration.

Some tests were made without side plates and the peak accelerations were about 30% less; however, these are not included here. All the results reported are with the plate

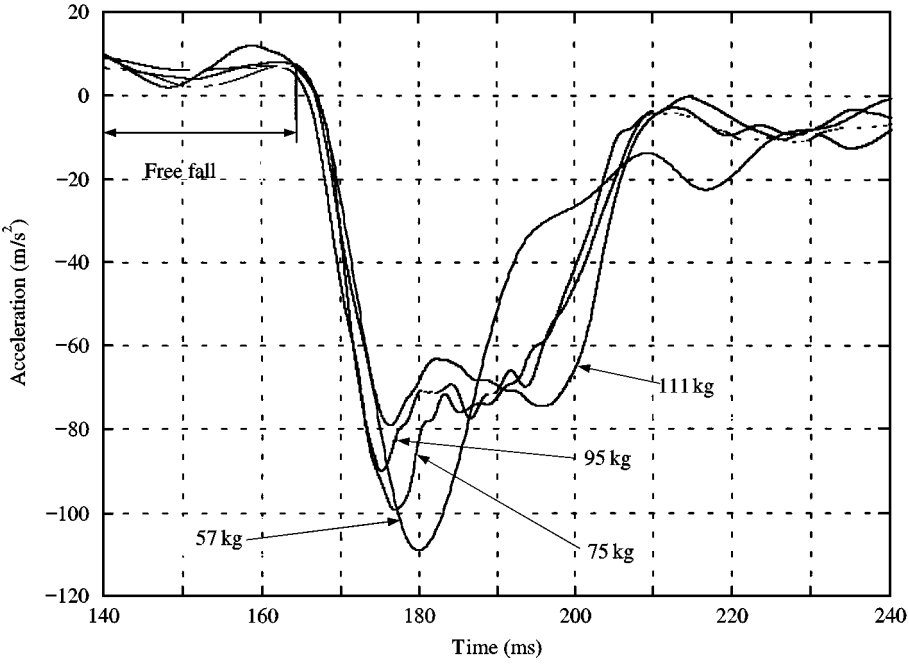

Figure 6. Comparison of typical accelerometer time histories for four different plate masses.

thoroughly dried. If the plate was wet the forces were consistently reduced by about 20%, indicating the possible effect of surface tension and/or surface roughness.

A high-speed video camera was used to visualize the flow at impact with the widest plate (without side plates). Recordings at 1000 frames per second were triggered by the photocell sensor. Four typical images at 2 ms intervals are shown in Figure 7 for a wave with $H/L = 0{\cdot}1$. The top frame is almost at the point of impact, and a jet has just started to form. The jets of water composed of small droplets of water may be seen below the plate on the left-hand side of the wave (travelling from right to left). A similar jet was not observed on the right-hand side of the wave. The front of the jet is travelling with a high velocity of about 30 m/s, although this may be much greater at the point of impact. An explosive sound was heard.

3. ANALYSIS

Figure 8 shows the velocity and angle of descent in a fixed frame of reference, V and α, respectively, and in the frame of reference relative to the wave, U and β, respectively. We assume that the vertical force depends on the water-surface shape, not the particle velocities in the wave, since water-particle velocities on impact are observed to be orders of magnitude greater. This implies that the velocity magnitude relative to the wave profile, U, and the angle of descent relative to the wave, β, are the important parameters. If we ignore the influence of surface tension and the compressibility of water, the parametric dependence of the slam force F_s may be stated as

$$F_s = F_s(\rho, m, U, \beta, g, H, L). \tag{1}$$

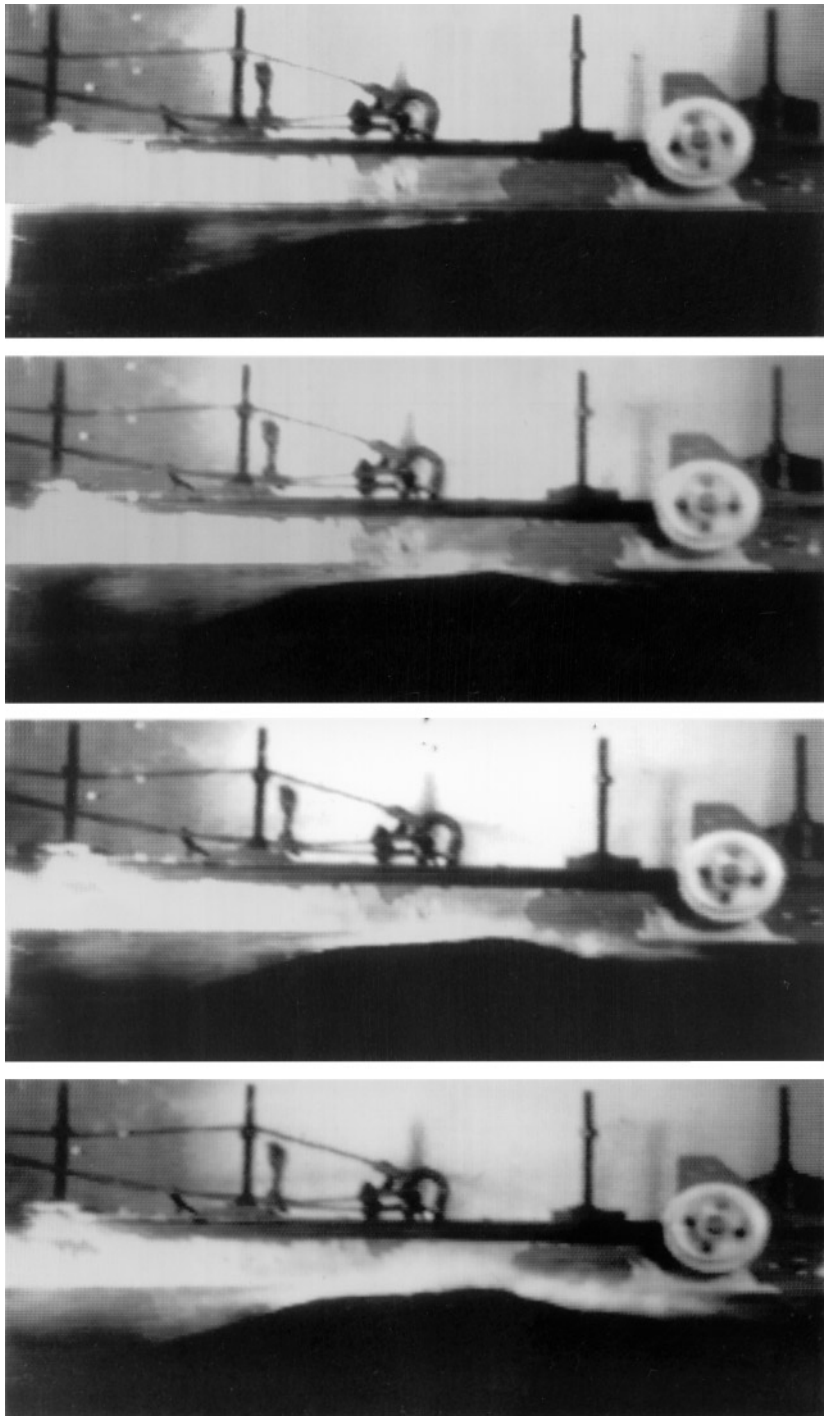

Figure 7. Frames from the high-speed video at 2 ms intervals (time increasing downwards) showing the jet forming on the left-hand side of the wave.

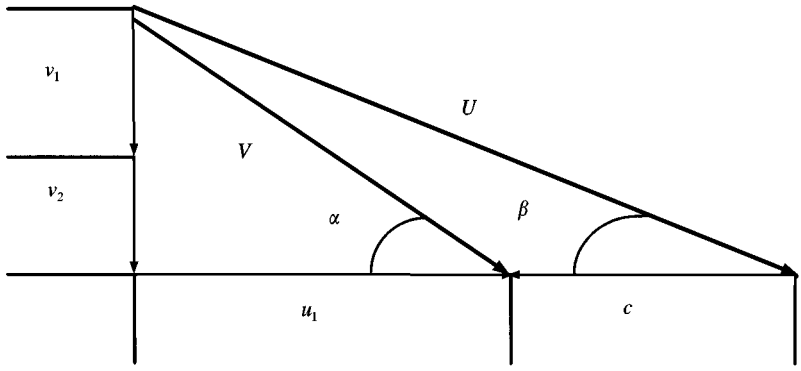

U = resultant velocity relative to wave
V = resultant velocity in fixed frame of reference.
v_1 = vertical velocity of body at bottom at track (from Photocell sensor).
v_2 = vertical velocity component due free-fall
u_1 = horizontal velocity of body at bottom of track
c = wave celerity

Figure 8. Velocity vector diagram for body at impact.

For convenience, with a plate of width b, we represent the mass m using a representative longitudinal length scale l of hydrodynamic impact at the time of maximum deceleration, such that

$$l = (m/\rho b)^{1/2}. \tag{2}$$

The slam force is nondimensionalized in the conventional way as a slam coefficient C_s:

$$C_s = \frac{F_s}{\frac{1}{2}\rho U^2 lb} = \frac{F_s}{\frac{1}{2}U^2\sqrt{\rho bm}}, \tag{3}$$

and the dependence may be reduced to

$$C_s = C_s\left(\beta, \frac{U}{\sqrt{gl}}, \frac{H}{L}, \frac{H}{l}\right). \tag{4}$$

The experiments show that dependence of C_s on $U/\sqrt{gl}$ and H/l is negligible. Furthermore, plotting C_s against β for different H/L, shown in Figure 9, suggests that the variables may be separated, such that

$$C_s = A\beta^B, \tag{5}$$

where $A = A(H/L)$, $B = B(H/L)$.

Plots of A against H/L and B against H/L are shown in Figure 10. Least-squares linear fits (shown in the figures) are given by

$$A = -97{\cdot}094\frac{H}{L} + 14{\cdot}389, \qquad B = -4{\cdot}593\frac{H}{L} + 1{\cdot}909. \tag{6}$$

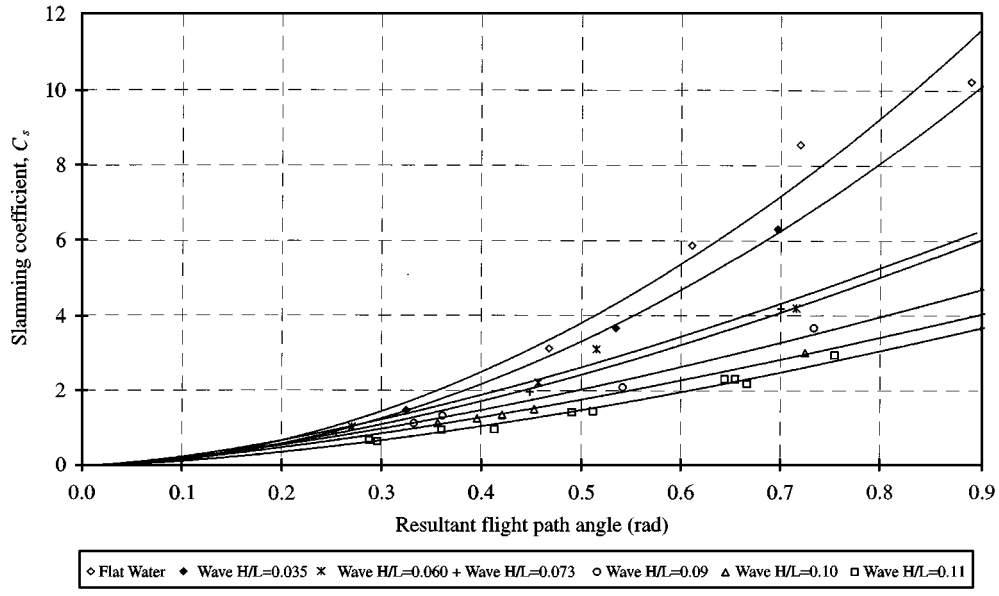

Figure 9. Plots of slam coefficient C_s against flight path angle (relative to wave profile) for various wave steepness H/L: ◇, flat water; ◆, wave $H/L = 0{\cdot}035$; *, $H/L = 0{\cdot}060$; +, $H/L = 0{\cdot}07$, ○ $H/L = 0{\cdot}090$; △, $H/L = 0{\cdot}100$; □, $H/L = 0{\cdot}110$.

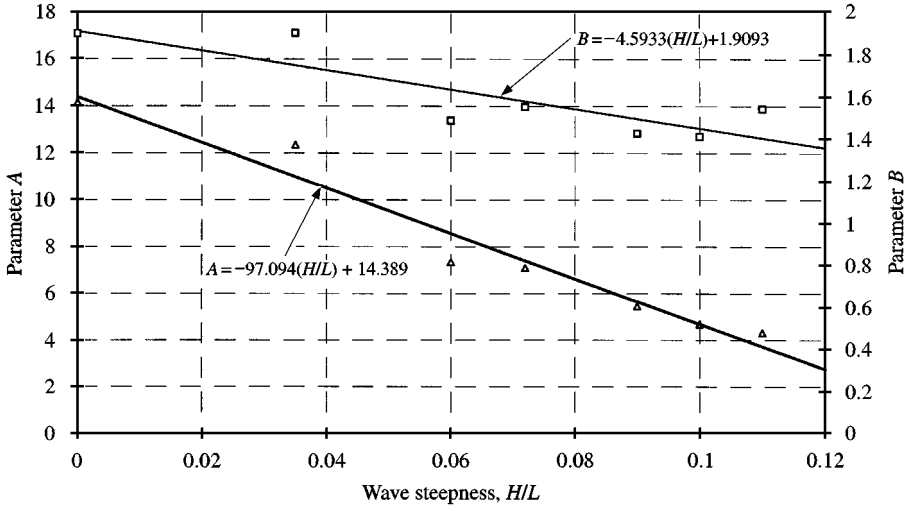

Figure 10. Plots of the parameters A and B in equation (5) against wave steepness H/L (with linear line fits); △, parameter A; □, parameter B.

Figure 11 shows the variation with H/L of the ratio of C_s given by formula (5), C_{ST}, to that measured directly, C_S. It is particularly noticeable that the formula consistently overestimates with $H/L = 0$ when air compressibility might be expected to be most significant. However, the correlation is 0.986 overall and the 95% confidence interval is 1.062 ± 0.038.

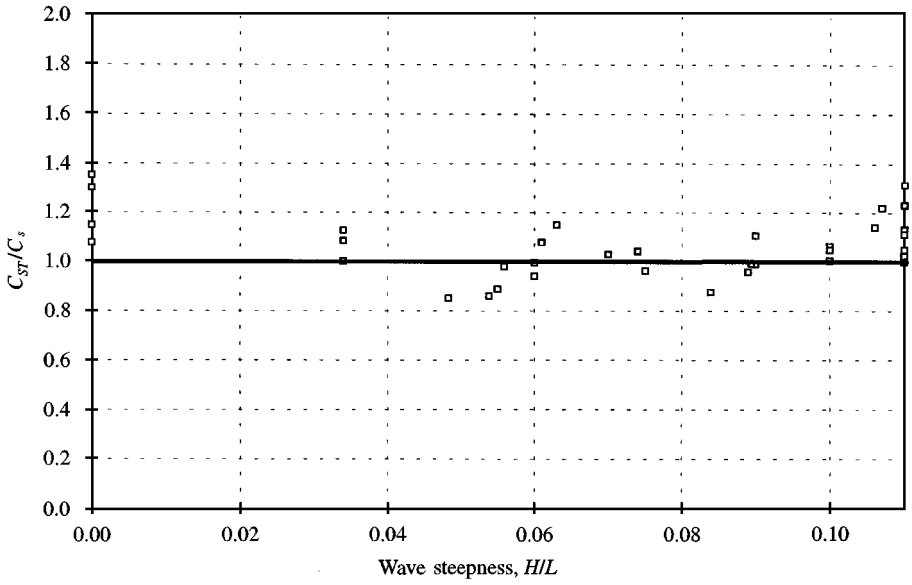

Figure 11. Plot of the ratio of the slam coefficient formula, equation (5), to experimental values, C_{ST}/C_S, against wave steepness H/L.

Nondimensionalizing using the vertical velocity at impact alone was also considered initially. This, however, did not collapse the data effectively, supporting the above assumption that the peak force is dependent on the motion of the body relative to the water mass in a vectorial sense.

It has been assumed that the depth of the water is large enough to have no influence on the slam force and that the depth of the side plates is large enough to produce two-dimensional flow in a vertical plane. Neither dimension was varied in the experiments, but some justification is provided by the results of pressure-impulse theory in Wood & Peregrine (1996), for a situation equivalent to a plate impacting flat water. They show that, if the depth of water is greater than about half the plate width, it has negligible effect on the results. Since the plate length in contact with water is less than 0·2 m at maximum deceleration and the water depth is greater than 0·5 m, the effect of water depth will be negligible. Also, the depth of the side plates is 0·1 m, representing a depth below the plate of at least one-half of a contact length at the plate, indicating that the water below the level of the side plates will have little effect on the plate.

The fine droplet structure of the jets at impact suggest that shocks may have been produced. However, the shock would be radiating through almost 180° from the region of impact and any reflection from the bed would cause further dispersion. Also, since the slam coefficient appears independent of water compressibility, its effect on slam force would appear to be insignificant.

Finally, it is interesting to compare with a large-scale result used as a basis for hovercraft design (British Hovercraft Safety Requirements 1992). Acceleration measurements were made on the SRN1, a hovercraft weighing 10 000 1b (4 545 kg), 9·1 m long and 7·3 m wide. The base of the hovercraft is the flat with flexible skirts. These will not make the flow two-dimensional, but the situation is somewhere between that with side plates and without

side plates in the experiments. The design formula for deceleration was based on measurements when the hovercraft speed was 15 and 20 m/s, the flight path angle 2·35° and $H/L = 0{\cdot}011$. Use of the slam coefficient formula (5) underpredicted deceleration by about 20%. Although the formula slightly overpredicts the experimental results for very small H/L (see Figure 11) and there is some uncertainty in the above values, this result may be considered to be of the same order as that deduced from the experimental results. The value of $U/\sqrt{gl}$ varied between about 2 and 5 in the experiments and is about 7 in the SRN1 case.

Fuller details of design calculations and the experimental rig and procedures are available in Smith (1997).

4. CONCLUSIONS

The maximum vertical slam force determined from the experiments has been shown to be defined to reasonable accuracy by a slam force coefficient as a function of wave steepness (H/L) and angle of descent relative to the wave (β) for the range of parameters tested. The coefficient showed no significant dependence on acceleration due to gravity, the compressibility of water and air and surface tension.

However, it should be stressed that while these experiments produce a remarkable well-defined result for maximum slam coefficient, the detailed nature of the physical processes remains poorly understood, particularly in relation to the compressibility of air (and possibly water), surface tension and water aeration. Simply having a wet rather than a dry plate surface significantly affects the maximum slam force.

The high-velocity jets produced by impact have a fine droplet structure, possibly generated by a shock wave in the water. There was an explosive sound at impact.

Some preliminary results for a sphere impacting a wave crest in the same rig under a similar range of conditions indicate that a slam coefficient based on similar dimensional reasoning describes experimental measurements rather well. In this case the jet at impact had a continuous, rather than a fine-droplet, structure and there was no explosive sound.

ACKNOWLEDGEMENTS

The high-speed video camera was loaned by the Rutherford Appleton Laboratory. Neil Smith was funded by the EPSRC Eng.D. scheme.

References

Ando, S. 1989 Cushioning of slamming impact by elastomeric layers. *Journal of Ship Research* **33,** 169–175.

Batterson, S. A. 1951 Water landing investigation of a hydro-ski model at beam loadings of 18·9 and 4·4. NACA RM L51F27.

British Hovercraft Safety Requirements 1992 Sub-section B4.2 (Issue 1, 1972, revised 1992). Civil Aviation Authority, U.K.

Cooker, M. J. & Peregrine, D. H. 1995 Pressure-impulse theory for liquid impact problems. *Journal of Fluid Mechanics* **297,** 193–214.

Crewe, P. 1960 Analysis of further deceleration measurements on the SRN1 hovercraft when flying over ship's wakes, ditching and flying over waves, Saunders-Roe Ltd. Hydrodynamics Note PRC/DGG/MFKI/3823.

Dobrovol'skaya, Z. N. 1969 On some problems of similarity flow of fluid with a free surface, *Journal of Fluid Mechanics* **36,** 805–829.

Greenhow, M. 1987 Wedge entry into initially calm water. *Applied Ocean Research* **9,** 214–223.

Greenhow, M. & Yanbao, L. 1987 Added mass for circular cylinders near or penetrating fluid boundaries – review, extension and application to water entry, exit and slamming. *Ocean Engineering* **14,** 325–348.

Korobkin, A. 1996 Global characteristics of jet impact. *Journal of Fluid Mechanics* **307,** 63–84.

Peregrine, D. H. & Thais, L. 1996 The effect of entrained air in violent water impacts. *Journal of Fluid Mechanics* **325,** 377–397.

Smith, N. J. 1997 Development of a highly manoeuvrable multirole amphibious vehicle. Eng.D. thesis, University of Manchester, U.K.

Verhagen, J. H. G. 1967 The impact of a flat plate on a water surface. *Journal of Ship Research* **9,** 211–223.

Von Karman, T. 1929 The impact of seaplane floats during landing. NACA TN 321, Washington, U.S.A.

Wagner, H. 1932 Uber stoss und gleitvorgange an der oberflache von flussigkeiten. *Zeitschrift für angewandte Mathematik und Mechanik* **12,** 193–215.

Wood, D. J. & Peregrine, D. H. 1996 Wave impact beneath a horizontal surface. *Proceedings* 25*th International Conference on Coastal Engineering*, Orlando, Florida, U.S.A. 2573–2583.

Zhao, R. & Faltinsen, O. 1992 Slamming loads on high-speed vessels. *Proceedings* 19*th ONR Conference*, Korea, Washington DC: Academic Press.

Zhao, R. & Faltinsen, O. 1993 Water entry of two-dimensional bodies. *Journal of Fluid Mechanics* **246,** 593–612.